Research Article

Journal of PeptideScience

Received: 23 June 2008 Revised: 27 November 2008 Accepted: 02 December 2008 Published online in Wiley Interscience: 10 February 2009

(www.interscience.com) DOI 10.1002/psc.1114

Synthetic pentapeptides inhibiting autophosphorylation of insulin receptor in a non-ATP-competitive mechanism

Masaki Kato,[a] Mineo Abe,[a] Yoshihiro Kuroda,[b]* Munetaka Hirose,[c] Minoru Nakano[a] and Tetsurou Handa[a]

In an attempt to develop non-ATP-competitive inhibitors of the autophosphorylation of IR, the effects of the synthetic peptides, Ac-DIY^{1158}ET-NH$_2$ and Ac-DY^{1162}Y^{1163}RK-NH$_2$, on the phosphorylation of IR were studied *in vitro*. The peptides were derived from the amino-acid sequence in the activation loop of IR. They inhibited the autophosphorylation of IR to 20.5 and 40.7%, respectively, at 4000 μM. The Asp/Asn- and Glu/Gln-substituted peptides, Ac-NIYQT-NH$_2$ and Ac-NYYRK-NH$_2$, more potently inhibited the autophosphorylation than did the corresponding parent peptides. The inhibitory potencies of the substituted peptides were decreased with increasing concentrations of ATP, indicating that these peptides employ an ATP-competitive mechanism in inhibiting the autophosphorylation of IR. In contrast, those of the parent peptides were not affected. Mass spectrometry showed that the parent peptides were phosphorylated by IR, suggesting that they interact with the catalytic loop. Moreover, docking simulations predicted that the substituted peptides would interact with the ATP-binding region of IR, whereas their parent peptides would interact with the catalytic loop of IR. Thus, Ac-DIYET-NH$_2$ and Ac-DYYRK-NH$_2$ are expected to be non-ATP-competitive inhibitors. These peptides could contribute to the development of a drug employing a novel mechanism. Copyright © 2009 European Peptide Society and John Wiley & Sons, Ltd.

Keywords: insulin receptor; phosphorylation; autoinhibition; non-ATP-competitive; peptide inhibitor

Introduction

RTKs play an important role in the regulation of most fundamental cellular processes such as proliferation, differentiation, migration, and metabolism [1–3]. Uncontrolled and elevated RTK activity resulting from overexpression is associated with a range of human malignant tumors [3,4]. Inhibition of these receptors therefore represents a potent approach for the treatment of various cancers.

IR is an $\alpha 2\beta 2$ heterotetrameric transmembrane protein possessing intrinsic tyrosine kinase activity [5]. Binding of insulin to the α-subunit elevates tyrosine-specific phosphotransferase activity, which leads to the autophosphorylation of specific tyrosine residues, called 'autophosphorylation sites', in the cytoplasmic β-subunit of IR. The autophosphorylation sites, which are mainly responsible for the activation of substrates, consist of three tyrosine residues (Tyr1158, Tyr1162, and Tyr1163) on the activation loop in the kinase domain [6]. The autophosphorylation sites recruit signaling proteins such as IR substrate-1, Shc, and Grb2. IR activates them, and then stimulates multiple intracellular signaling cascades such as the PI(3)K pathway, CAP/Cbl pathway, and Ras/MAPK pathway, which induce glucose metabolism, protein synthesis, and cell proliferation [7,8].

The kinase activities of RTKs have unique regulation. In the inactive state, some domains of RTKs bind to their own kinase domains and kinase activities are suppressed [9]. Binding of an intrinsic ligand molecule to inactive RTK leads to conformational change of RTK, followed by the activation of RTK and phosphorylation of substrates. The details of the autoinhibition mechanisms of several RTKs have been clarified. The *C*-terminal tails of Tie2 kinase [10], PDGFR [11], VEGFR-2 [12], and RON kinase [13] interact with their kinase domains and inhibit their own activities. On the other hand, the activity of Ephb2 receptor is regulated by its own juxtamembrane region [14]. The activation loop in IRK autoinhibits kinase activity by binding to its own catalytic region [15–17]. In an inactive state, the catalytic loop of IR (H^{1130}RDLAARN^{1137}), which plays a crucial role in phosphotransfer reactions, is hidden by the activation loop. Once three tyrosine residues in the activation loop (Tyr1158, Tyr1162, and Tyr1163) are phosphorylated, the activation loop dissociates from the catalytic loop with ligand-stimulated conformational change of the β-subunit. The catalytic loop exposed to solvent can phosphorylate the autophosphorylation sites (Tyr965, Tyr972, Tyr1158, Tyr1162, Tyr1163, Tyr1328, and Tyr1334) of another β-subunit in a *trans* manner and IR is activated.

* *Correspondence to: Yoshihiro Kuroda, Faculty of Pharmaceutical Sciences, Himeji Dokkyo University, Himeji, Hyogo 670-8524, Japan. E-mail: yokuroda@himeji-du.ac.jp*

a *Graduate School of Pharmaceutical Sciences, Kyoto University, Sakyo-ku, Kyoto 606-8501, Japan*

b *Faculty of Pharmaceutical Sciences, Himeji Dokkyo University, Himeji, Hyogo 670-8524, Japan*

c *Department of Anesthesiology and Reanimatology, Faculty of Medicine, Fukui University, Eiheiji-cho, Yoshida-gun, Fukui 910-1193, Japan*

Abbreviations used: *IR, insulin receptor; RTK, receptor tyrosine kinase; IRK, the kinase domain of IR; EGFR, epidermal growth factor receptor; EGF, epidermal growth factor; pY, phosphotyrosine; pTyr, phosphotyrosine;HEPES, 2-[4-(2-Hydroxyethyl)-1-piperazyl] ethanesulfonic acid;PVDF, polyvinylidine difluoride.*

Previously, we found that a pentapeptide, Ac-DIYET-NH_2, inhibits the autophosphorylation of IR [18]. The peptide includes the amino-acid sequence around an autophosphorylation site (Tyr1158) in the activation loop of IR (G^{1149}DFGMTRDIY^{1158}ETD$Y^{1162}Y^{1163}$RKGGKGL^{1170}). We focused on the other autophosphorylation sites in the activation loop, i.e. Tyr1162 and Tyr1163, and synthesized a peptide, Ac-DYYRK-NH_2, which consists of the amino-acid sequence around these autophosphorylation sites. In this study, we investigated the effects of Ac-DIYET-NH_2, Ac-DYYRK-NH_2, and their modified peptides on the autophosphorylation of IR. Moreover, inhibition mechanisms by the peptides, which were not proved in the previous study, are also investigated and discussed.

Materials and Methods

Materials

Antiphosphotyrosine antibody 4G10 was obtained from Upstate Biotechnology (Lake Placid, NY). Purified IR from rat liver, purified EGFR from human carcinoma A431 cells, insulin, and EGF were obtained from Sigma Chemical (St Louis, MO). All Fmoc-L-amino acids were purchased from the Peptide Institute (Osaka, Japan), except Fmoc-L-Tyr{PO(OBzl)OH}-OH, which was from Watanabe Chemical Industries (Hiroshima, Japan).

Synthesis and Purification of Peptides

Peptides were synthesized automatically by the solid-phase method using Fmoc chemistry on an ABI 433A Peptide Synthesizer (Applied Biosystems, Foster, CA). Their *N*-termini were acetylated (Ac-) and *C*-termini were amidated (–NH_2). After cleavage with TFA, the peptides were purified on a reverse phase C_{18} HPLC column (Waters, Milford, MA) using a gradient from 100% A, 0% B to 60% A, 40% B in 40 min, where A is 0.1% TFA in water and B is 0.1% TFA in acetonitrile. The peptides were characterized by mass spectrometry using a Sciex API III Mass Spectrometer (PerkinElmer Life and Analytical Sciences, Wellesley, MA) and Mariner-E Biospectrometry Workstation (PerSeptive Biosystems, Framingham, MA). Ac-DIYET-NH_2: *m/z* calculated 680.30 (monoisotope), 680.70 (average), found 681.5 ($[M + H]^+$); Ac-DYYRK-NH_2: *m/z* calculated 784.39 (monoisotope), 784.86 (average), found 785.5 ($[M + H]^+$); Ac-DIAET-NH_2: *m/z* calculated 588.28 (monoisotope), 588.61 (average), found 589.2 ($[M + H]^+$); Ac-DAARK-NH_2: *m/z* calculated 600.33 (monoisotope), 600.67 (average), found 601.2 ($[M + H]^+$); Ac-DIFET-NH_2: *m/z* calculated 664.31 (monoisotope), 664.70 (average), found 665.3 ($[M + H]^+$); Ac-DFFRK-NH_2: *m/z* calculated 752.40 (monoisotope), 752.86 (average), found 753.4 ($[M + H]^+$); Ac-DIpYET-NH_2: *m/z* calculated 760.27 (monoisotope), 760.68 (average), found 761.3 ($[M + H]^+$); Ac-DpYpYRK-NH_2: *m/z* calculated 944.32 (monoisotope), 944.82 (average), found 946.3 ($[M + H]^+$); Ac-NIYQT-NH_2: *m/z* calculated 678.33 (monoisotope), 678.73 (average), found 679.5 ($[M + H]^+$); Ac-NYYRK-NH_2: *m/z* calculated 783.40 (monoisotope), 783.87 (average), found 784.5 ($[M + H]^+$).

In Vitro Phosphorylation of IR in the Presence of Synthetic Peptides

Purified IR (4.1 μg/ml) was phosphorylated with or without 2.6-μg/ml insulin and synthetic peptides for 10 min at 37 °C in 50 μl of incubation buffer, including 50-mM HEPES, pH 7.4, 125-mM NaCl, 1-mM EDTA, 10-mM $MgCl_2$, 5-mM $MnCl_2$, 5-mM dithiothreitol, 1-mM phenylmethylsulfonyl fluoride, and ATP. The concentration of ATP was 20 μM unless otherwise noted. After the reactions were stopped by the addition of Laemmli sample buffer and boiling for 5 min, IRs were separated by SDS-PAGE in 7.5% (v/v) acrylamide gels and transferred to a PVDF membrane (GE Healthcare Bio-Sciences, Piscataway, NJ). The membranes were blocked in 1% (w/v) BSA in tris buffered saline–0.1% Tween 20 at room temperature overnight, and then immunoblotted with antiphosphotyrosine antibody 4G10. The antigen–antibody complexes were visualized with western blotting luminol reagent (Santa Cruz Biotechnology, Santa Cruz, CA). The bands were exposed to X-ray films (Fuji Photo Film, Tokyo, Japan) and images were analyzed by Scion Image 4.0.2 (Scion, Frederick, MD).

In Vitro Phosphorylation of EGFR in the Presence of Synthetic Peptides

Purified EGFR (1.9 μg/ml) was phosphorylated with or without 10-μg/ml EGF and synthetic peptides for 10 min at 37 °C in 50 μl of the incubation buffer including 20-μM ATP. After the reactions were stopped by the addition of Laemmli sample buffer and boiling for 5 min, EGFRs were separated by SDS-PAGE, followed by immunoblot analysis with antiphosphotyrosine antibody 4G10.

Statistical Analysis

Experimental data were analyzed by one-way analysis of variance with Dunnett's *post hoc* analysis. Statistical significance was established at $P < 0.05$. All values are reported as the means ± standard deviations.

Studies on Phosphorylation of Synthetic Peptides by Mass Spectrometry

Purified IR (41 μg/ml) was incubated for 30 min at 37 °C with 2.6 μg/ml insulin, 20-μM ATP, 1-μM DIYET, 1-μM DYYRK, 1-μM NIYET, and 1-μM NYYRK. The reaction mixture was desalted with the solid-phase extraction method using Discovery DSC-18 (Supelco, Bellefonte, PA). The eluent was 75% A, 25% B for DIYET, 80% A, 20% B for DYYRK, 70% A, 30% B for NIYQT, or 60% A, 40% B for NYYRK, where A is 0.1% TFA in water and B is 0.1% TFA in acetonitrile. The molecular masses of peptides in the sample solution were analyzed with a Sciex API III Mass Spectrometer and Mariner-E Biospectrometry Workstation.

System Setup for Docking Simulations

The X-ray structure of IRK [16], which is 303 amino acids long (Ser981–Lys1283) and bound with an ATP analog and a peptide substrate, was from the RCSB Protein Data Bank [19]. The PDB ID is 1IR3. Coordinate files of the synthetic peptides, assuming an extended structure, were created using PyMOL v0.99 (DeLano Scientific LLC, South San Francisco, CA) [20]. Each was manually placed at the substrate-binding site of IRK using the UCSF Chimera package (The Resource for Biocomputing, Visualization, and Informatics at the University of California, San Francisco, CA) [21]. The direction of *N*- and *C*-termini of the peptide was the same as that of the peptide substrate. Charges of all the atoms were assigned and added according to the all atom charge model of AMBER 94 [22]. Hydrogen atoms were added with standard geometries.

Docking Simulations – GRID Scoring Function

The prepared coordinate files for docking simulations were processed by the DOCK Suite of Programs 6.1: SPHGEN, GRID, DOCK, and other accessories (URL: http://dock.compbio.ucsf.edu/; University of California, San Francisco, CA) [23,24]. A molecular surface was created for IRK using the DMS program (URL: http://www.cgl.ucsf.edu/Overview/software.html), and then used in SPHGEN to calculate spheres for docking [25]. Force field grids were calculated in GRID [26]. GRID scores are approximate interaction energies including van der Waals and electrostatic components:

$$\text{Score} = \sum_{i=1}^{\text{peptide}} \left(\sqrt{A_{ii}} \sum_{j=1}^{\text{IRK}} \frac{\sqrt{A_{ii}}}{r_{ij}^{12}} - \sqrt{B_{ii}} \sum_{j=1}^{\text{IRK}} \frac{\sqrt{B_{jj}}}{r_{ij}^{6}} + 332qi \sum_{j=1}^{\text{IRK}} \frac{q_j}{Dr_{ij}} \right) \quad (1)$$

Each term is a double sum over the peptide atoms i and IRK atoms j. A and B are van der Waals repulsion and attraction parameters, respectively. The distance in Å between atoms i and j is r_{ij}. The point charges on atoms i and j are q_i and q_j. Equation (1) does not contain an explicit hydrogen-bonding term. We assume that hydrogen bond energies can largely be accounted for in the electrostatic term. A 10-Å cutoff and a dielectric function of $D = 4r_{ij}$ were used. Simulations of docking between IRK and the peptides were executed using the anchor and grow procedure [27] in DOCK.

Docking Simulations – AMBER Scoring Function

The results obtained from simulations using the GRID scoring function were further estimated by the AMBER scoring function, in which both the peptides and the interactive site of IRK can be flexible, allowing small structural rearrangements to reproduce the induced-fit while performing the scoring function. In AMBER scoring, the program performs minimization and molecular dynamics (MD) simulation on the peptide, IRK, and the complex individually, and calculates the score as follows:

$$\text{Score}\,(E_{\text{binding}}) = E_{\text{complex}} - (E_{\text{IRK}} + E_{\text{peptide}}) \quad (2)$$

where, E is the sum of AMBER MM potentials and solvation free energy derived from the generalized Born/surface area continuum model [28]. The atoms of IRK within 10 Å from the peptide were flexible. A modified GB (OBC) model [29] was used as the generalized Born model. Following 1000 minimization steps, 3000 MD steps (3 ps) were performed at a constant temperature of 310 K. The structures of the complex of the peptide and IRK having the most stable score were figured using PyMOL.

Results

Autophosphorylation of IR in the Presence of Synthetic Peptides *In Vitro*

We investigated the effects of synthetic peptides on the autophosphorylation of IR. The results at 20-μM ATP are shown in Figure 1, where the insulin-stimulated responses of IR without peptides at 10 min were taken as the control and considered to be 100%. DIYET and DYYRK inhibited the autophosphorylation of IR to 20.5 and 40.7% at 4000 μM, respectively (Figure 1(a) and (b), white bars). IC_{50} values of DIYET and DYYRK were 477.8 and 1228.8 μM, respectively. In the coexistence of DIYET and DYYRK, the inhibitory effects of these peptides decreased; the mixture inhibited the autophosphorylation of IR to 56.2% at 4000 μM each (Figure 1(c)). The results concerning the replacement of tyrosine residues in the peptides with alanine (Tyr/Ala), phenylalanine (Tyr/Phe), or phosphotyrosine (Tyr/pTyr) are shown in Figure 2, where the insulin-stimulated responses of IR without peptides at 10 min were taken as the control and considered to be 100%. The Tyr/Ala-substituted peptide, DIAET, and the Tyr/Phe-substituted peptides, DIFET and DFFRK, hardly inhibited the autophosphorylation of IR. The inhibitory potency of DAARK was weaker than that of its parent peptide, DYYRK. The inhibitory effects of the peptides, including phosphotyrosine, DIpYET and DpYpYRK, were much less than those of their parent peptides, DIYET and DYYRK, respectively; however, the inhibitory effect of DIpYET at low concentrations (40–400 μM) was more than that of DIYET.

Effects of Replacing Negatively Charged Amino Acids with Corresponding Neutral Amino Acids in the Peptides on Inhibitory Potencies

Figure 3 shows the effects of modified peptides in which aspartate and glutamate are replaced with asparagine (Asp/Asn) and glutamine (Glu/Gln), respectively, on the autophosphorylation of IR. The insulin-stimulated responses of IR without peptides at 10 min were taken as the control and considered to be 100%. The maximal concentration of NIYQT was 1000 μM because 4000-μM NIYQT was not completely dissolved. The inhibitory potencies of NIYQT and NYYRK at 20-μM ATP were greater than those of the parent peptides (Figure 3(a) and (b), white bars). IC_{50} values of NIYQT and NYYRK were 24.6 μM and 465.2 μM, respectively.

Effects of the Concentration of ATP on the Inhibitory Potencies of the Peptides

We examined the effects of the ATP concentration on the inhibitory potencies of the peptides. IR was incubated with the peptides at various concentrations of ATP (20 μM, 200 μM, and 2000 μM). DIYET and DYYRK were not affected by the concentration of ATP (Figure 1(a) and (b)). In contrast, the inhibitory effects of NIYQT and NYYRK significantly decreased as the concentration of ATP increased (Figure 3), indicating that these peptides are ATP-competitive inhibitors.

Effects of the Inhibitory Peptides on the Autophosphorylation of EGFR

In order to evaluate the selectivity of inhibitory peptides for IR, their effects on the autophosphorylation of EGFR, a popular RTK, were estimated (Figure 4). EGF-stimulated responses of EGFR without peptides at 10 min were taken as the control and considered to be 100%. The autophosphorylation of EGFR was significantly inhibited by NIYQT and NYYRK. On the other hand, DIYET hardly inhibited the autophosphorylation of EGFR and the inhibitory effect of DYYRK on EGFR was much less than that on IR.

Detection of Phosphorylated Peptides by Mass Spectrometry

In order to investigate whether the peptides are phosphorylated by IR as exogenous substrates, we measured mass spectra of DIYET, DYYRK, NIYQT, and NYYRK after incubation with IR, insulin, and ATP. The results are summarized in Tables 1 and 2. The corresponding ions due to the phosphorylated peptides were

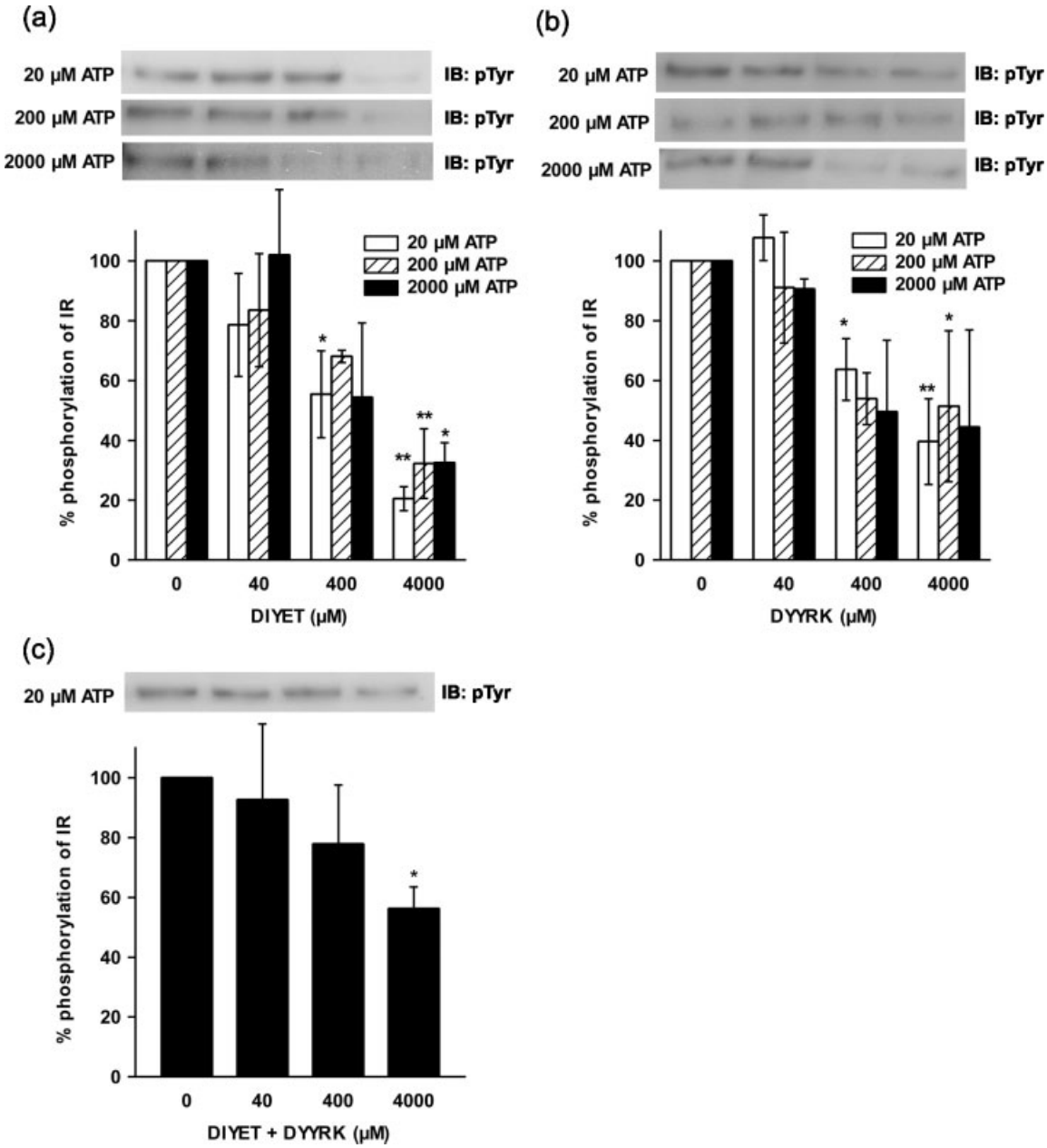

Figure 1. Phosphorylation of purified IR in the presence or absence of (a) DIYET, (b) DYYRK, and (c) a mixture of DIYET and DYYRK. IR was incubated with or without peptides for 10 min at 37 °C in buffer containing ATP. The concentration of ATP was 20, 200, or 2000 μM. Results displayed in the top panels represent typical immunoblots (IB). $^{*}P < 0.05$, $^{**}P < 0.01$ *versus* insulin-stimulated tyrosine phosphorylation at 10-min incubation without peptides; $n = 3–4$ for each lane.

detected for both DIpYET and DpYpYRK in negative-ion operation mode (Table 1 and Figure 5). Phosphorylated NIpYQT was also detected in positive-ion operation mode, while phosphorylated NpYpYRK was not found (Table 2). These results indicate that DIYET, DYYRK, and NIYQT were phosphorylated by IR.

Docking Simulations of Interactions between Inhibitory Peptides and IRK

We used DOCK 6 and its accessory programs in order to estimate the binding modes of the modified peptides, NIYQT and NYYRK, and their parent peptides, DIYET and DYYRK. Figure 6 shows schematically the initial position of peptides for docking simulations and the resulting locations of the peptides.

Table 1. Theoretical and observed *m/z* values for peptides in negative-ion mass spectra

	Theoretical (monoisotope)		Observed	
	$[M-H]^-$	$[M-2H]^{2-}$	$[M-H]^-$	$[M-2H]^{2-}$
DIYET	679.29	339.14	N.D.	N.D.
DIpYET	759.26	379.13	N.D.	379.0
DYYRK	783.38	391.19	N.D.	N.D.
DpYYRK or DYpYRK	863.35	431.17	N.D.	N.D.
DpYpYRK	943.31	471.15	N.D.	471.0

N.D., not detected.

Journal of PeptideScience

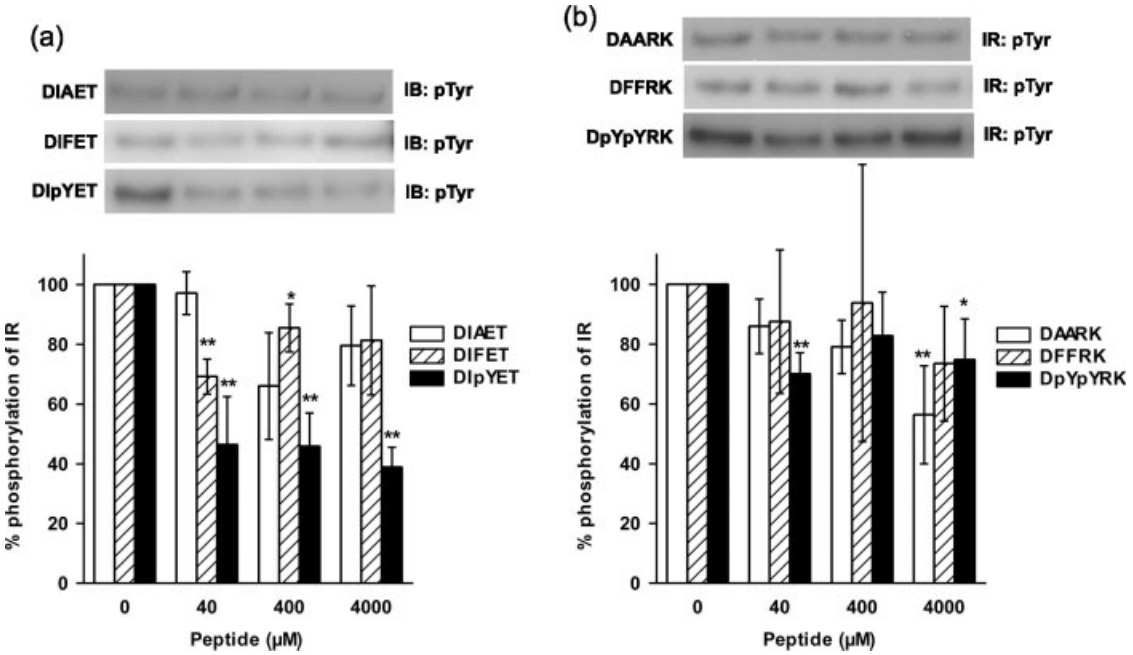

Figure 2. Phosphorylation of purified IR in the presence or absence of peptides in which tyrosine residue is replaced with alanine, phenylalanine, or phosphotyrosine. The corresponding parent peptides are (a) DIYET and (b) DYYRK. IR was incubated with or without peptides for 10 min at 37 °C in the buffer containing 20 μM of ATP. Results displayed in the top panels represent typical immunoblots (IB). $^{*}P < 0.05$, $^{**}P < 0.01$ *versus* insulin-stimulated tyrosine phosphorylation at 10-min incubation without peptides; $n = 4$ for each lane.

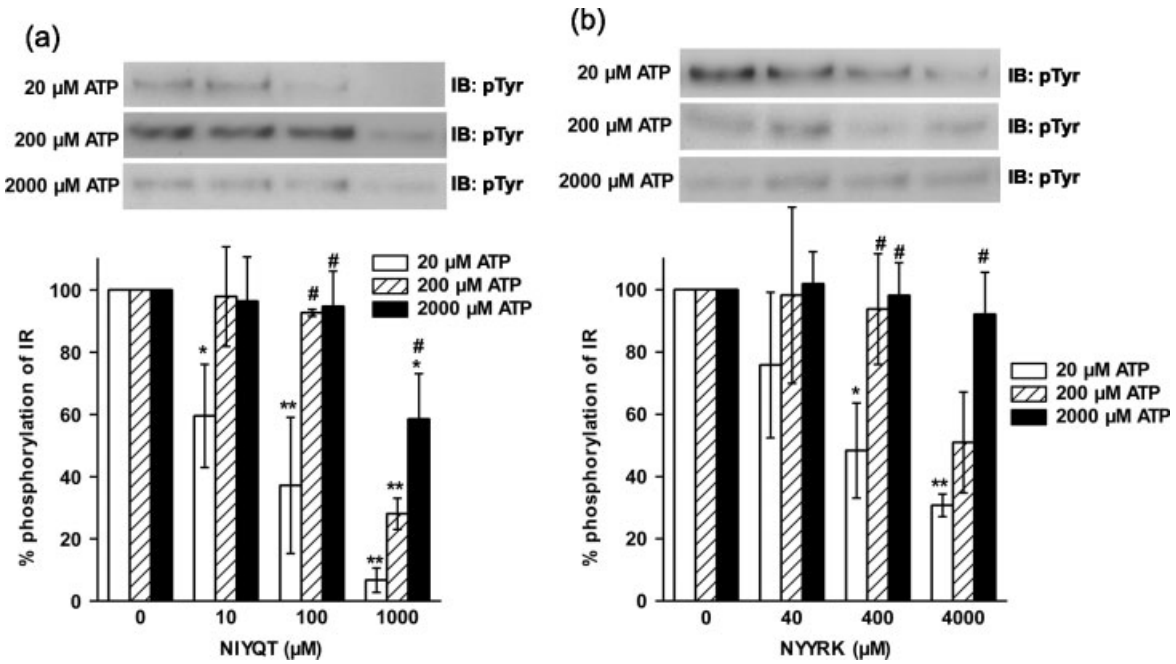

Figure 3. Phosphorylation of purified IR in the presence or absence of (a) NIYQT or (b) NYYRK. IR was incubated with or without peptides for 10 min at 37 °C in the buffer containing ATP. The concentration of ATP was 20, 200, or 2000 μM. Results displayed in the top panels represent typical immunoblots (IB). $^{*}P < 0.05$, $^{**}P < 0.01$ *versus* insulin-stimulated tyrosine phosphorylation at 10-min incubation without peptides; $\#P < 0.05$ *versus* tyrosine phosphorylation at 20 μM ATP; $n = 3$ for each lane.

Because we expected some inhibitory peptides to bind to the substrate-binding site in IRK, the initial position of the four peptides was set at the substrate-binding site, which is surrounded by αEF (Pro1178–Asp1183), αG (Asn1215–Met1223), β11 (Leu1170–Leu1171), P + 1 loop (Leu1171–Ala1177), and the catalytic loop (His1130–Asn1137) [16].

Fifty conformations of each peptide were obtained from docking simulation using GRID scoring function. They did not converge at a single position (the mean global root mean square deviations (RMSD) value of 50 conformations, DIYET: 9.96 ± 5.20 Å; DYYRK: 7.48±2.56 Å; NIYQT: 7.61±4.21 Å; NYYRK: 6.73±4.43 Å). Figure 7 shows the calculated conformations of DIYET using GRID scoring

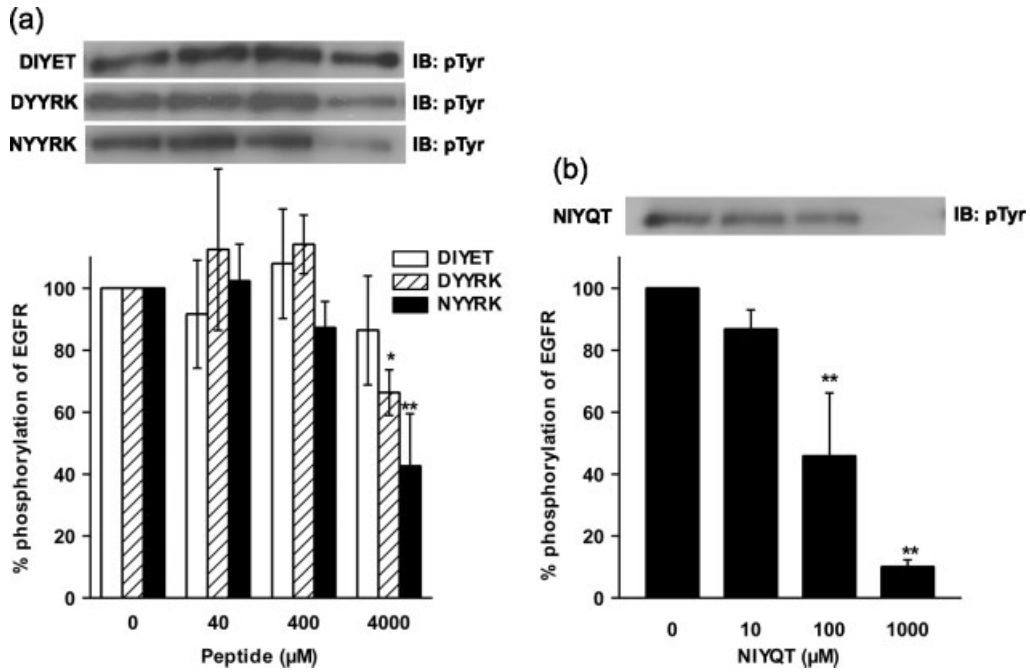

Figure 4. Phosphorylation of purified epidermal growth factor receptor (EGFR) in the presence or absence of (a) DIYET (white bars), DYYRK (shaded bars), NYYRK (black bars), or (b) NIYQT. IR was incubated for 10 min at 37 °C in buffer containing 20 μM ATP. Results displayed in the top panels represent typical immunoblots (IB). $^{*}P < 0.05$, $^{**}P < 0.01$ *versus* EGF-stimulated tyrosine phosphorylation at 10-min incubation without inhibitors; $n = 4$ for each lane.

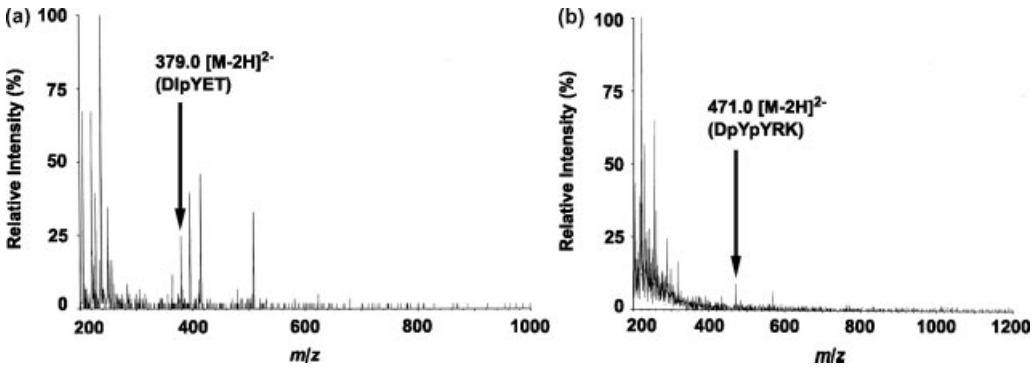

Figure 5. Mass spectra of the solutions for mixtures of DIYET and DYYRK incubated with IR, insulin, and ATP. The reaction mixture was desalted with the solid-phase extraction method. (a) Negative-ion mode mass spectrum of the eluent for DIYET (75% A, 25% B), (b) negative-ion mode mass spectrum of the eluent for DYYRK (80% A and 20% B). A is 0.1% TFA in water and B is 0.1% TFA in acetonitrile.

Table 2. Theoretical and observed *m/z* values for peptides in positive-ion mass spectra

	Theoretical (monoisotope)		Observed	
	$[M + H]^+$	$[M + 2H]^{2+}$	$[M + H]^+$	$[M + 2H]^{2+}$
NIYQT	679.34	340.17	N.D.	340.0
NIpYQT	759.31	380.16	N.D.	380.2
NYYRK	784.41	392.70	N.D.	392.6
NpYYRK or NYpYRK	864.38	435.57	N.D.	N.D.
NpYpYRK	944.34	472.68	N.D.	N.D.

N.D., not detected.

function. The conformations of the other peptides were similar to Figure 7. Their scores (energy) were also distributed in a large range. We analyzed their scores and estimated occupancy of each conformation according to the Boltzmann distribution. The Boltzmann distribution is expressed as

$$\theta_i = \frac{\exp(-\beta\varepsilon_i)}{\sum_j \exp(-\beta\varepsilon_i)} \quad \beta = \frac{1}{kT} \tag{3}$$

where θ is occupancy of a conformation, ε is average energy of a conformation, k is the Boltzmann constant, T is the thermodynamic temperature, and $\Sigma_j \exp(-\beta\varepsilon_j)$ is the partition function. In this case, the GRID score is substituted for ε. We adopted the conformation of each peptide which has the best score (the lowest energy) because their occupancy was nearly 100% except for NIYQT (Table 3). The occupancy of NIYQT is 86.3%. Subsequently, the peptides having the adopted conformations and IRK were simulated together using AMBER scoring function to obtain the induced-fit structures.

Journal of PeptideScience

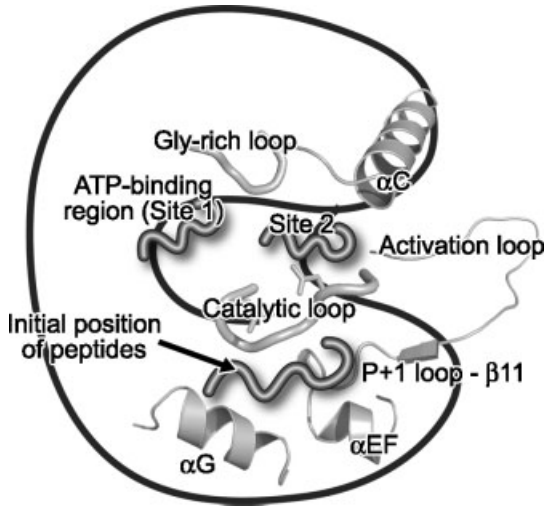

Figure 6. Schematic drawing of the initial position of a peptide for docking simulations and the resulting locations (Site 1 and Site 2) of the peptide in the kinase domain of IR. The crucial regions described in the text are labeled. The initial position of all peptides was set as the substrate-binding site surrounded by αEF (Pro1178–Asp1183), αG (Asn1215–Met1223), β11 (Leu1170-Leu1171), P + 1 loop (Leu1171-Ala1177), and the catalytic loop (His1130–Asn1137). Site 1 represents the ATP-binding region and Site 2 represents a region surrounded by αC (Leu1038–Met1051), the Gly-rich loop (Gly1003–Gly1008), and the catalytic loop.

Table 3. Occupancy of the conformation of each peptide which has the best score estimated according to the Boltzmann distribution

	The best score (J)	Boltzmann factor $[\exp(-\beta\varepsilon_i)]$	Partition function $[\Sigma_j \exp(-\beta\varepsilon_j)]$	Occupancy
DIYET	-5.437×10^{-19}	1.395×10^{55}	1.395×10^{55}	~1.000
DYYRK	-6.798×10^{-19}	8.729×10^{68}	8.731×10^{68}	0.9998
NIYQT	-5.185×10^{-19}	3.897×10^{52}	4.516×10^{52}	0.8629
NYYRK	-6.108×10^{-19}	8.910×10^{61}	8.910×10^{61}	~1.000

The simulation showed that the binding sites of the inhibitory peptides are roughly classified into two sites: the ATP-binding region (Site 1) and a region surrounded by αC (Leu1038–Met1051), the Gly-rich loop (Gly1003–Gly1008), and the catalytic loop (Site 2). The ATP-binging region consists of the adenine-binding region (Val1010, Glu1077, Met1079, and Met1139) and the amino-acid residues essential to binding the phosphate groups of ATP (Ser1006 and Lys1030). We analyzed hydrogen bonds and salt bridges between the peptides and IRK in the complex having the most stable score by geometric analysis [30].

DIYET, the parent peptide, was located at Site 2 and Thr5 was positioned near Asp1132 and Arg1136 in the catalytic loop (Figure 8(a)), which plays a crucial role in phosphate transfer from ATP to the autophosphorylation sites and substrates [17,31]. The Glu4 side chain was within hydrogen-bonding distance for the terminal two nitrogen atoms of the Arg1136 side chain (2.8 Å). These results indicate that DIYET would prevent a substrate from accessing the catalytic loop.

DYYRK, the parent peptide, was located at Site 2, while its *N*-terminal moiety was located at Site 1 (Figure 8(b)). The aromatic ring of Tyr2 and Tyr3 covered Asp1132 and Arg1136 in the catalytic loop. The Tyr2 side chain could form a hydrogen bond with the Lys1085 side chain (3.0 Å), which has an important role in substrate binding. These results indicate that DYYRK would inhibit substrate binding to the catalytic loop of IR.

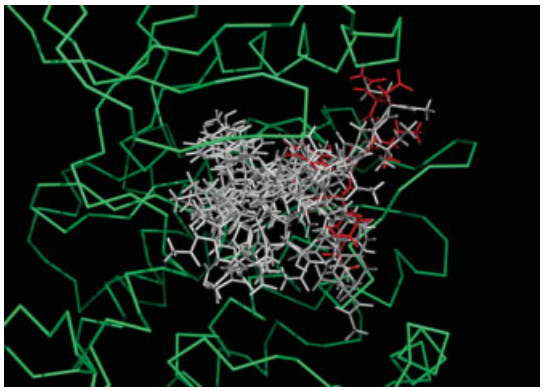

Figure 7. Conformations of DIYET calculated using GRID scoring function. Ten conformations that have lower energy are overlaid as line models and the most stable conformation is colored in red. The backbone of the kinase domain of IR are displayed as a green line.

NIYQT was located at Site 1 (Figure 8(c)). The Thr5 side chain was positioned at the ATP-binding region. The Gln4 backbone and side chain could form hydrogen bonds with the Lys1030 side chain (2.9 Å) and the Arg1136 backbone (2.8 Å), respectively, which play a crucial role in binding the phosphate group of ATP. It is presumed that NIYQT would inhibit the autophosphorylation of IR in an ATP-competitive manner.

While part of the *N*-terminal moiety of NYYRK is positioned at Site 2, its major part was located at Site 1 (Figure 8(d)). The aromatic ring of Tyr2 was occupied at the binding site of the ribose ring of ATP. The acetyl group of the peptide could form a hydrogen bond with the Ser1006 backbone (2.9 Å), which is involved in binding the phosphate group of ATP. These results suggest that NYYRK inhibits the autophosphorylation of IR in an ATP-competitive manner.

Discussion

It has been reported that overexpression of IR triggers most human breast cancers [32]. Both ligand-dependent malignant transformation and increased cell growth occur in cultured breast cells overexpressing IR; therefore, inhibitors of IR activity could contribute to the development of a novel anticancer drug. In this study, we found that several peptides inhibited the activity of IR. These inhibitory peptides have potential as seed compounds for anticancer drugs.

DIYET and DYYRK, which include the amino-acid sequences of the activation loop of IR, inhibited the autophosphorylation of IR (Figure 1). In the coexistence of these peptides, inhibitory potencies decreased. This result indicates that these peptides do not cooperate and would interact with the same region of IR. We presumed that tyrosine residues in the peptides are essential for the inhibitory effects. To characterize the inhibitory effects of the peptides in detail, we replaced tyrosine residues in the peptides with alanine (Tyr/Ala), phenylalanine (Tyr/Phe) or phosphotyrosine (Tyr/pTyr) and investigated the effects of the substituted peptides on the autophosphorylation of IR. Tyr/Ala- and Tyr/Phe-substituted peptides lost their inhibitory potencies (Figure 2), indicating that tyrosine residues in the peptides play

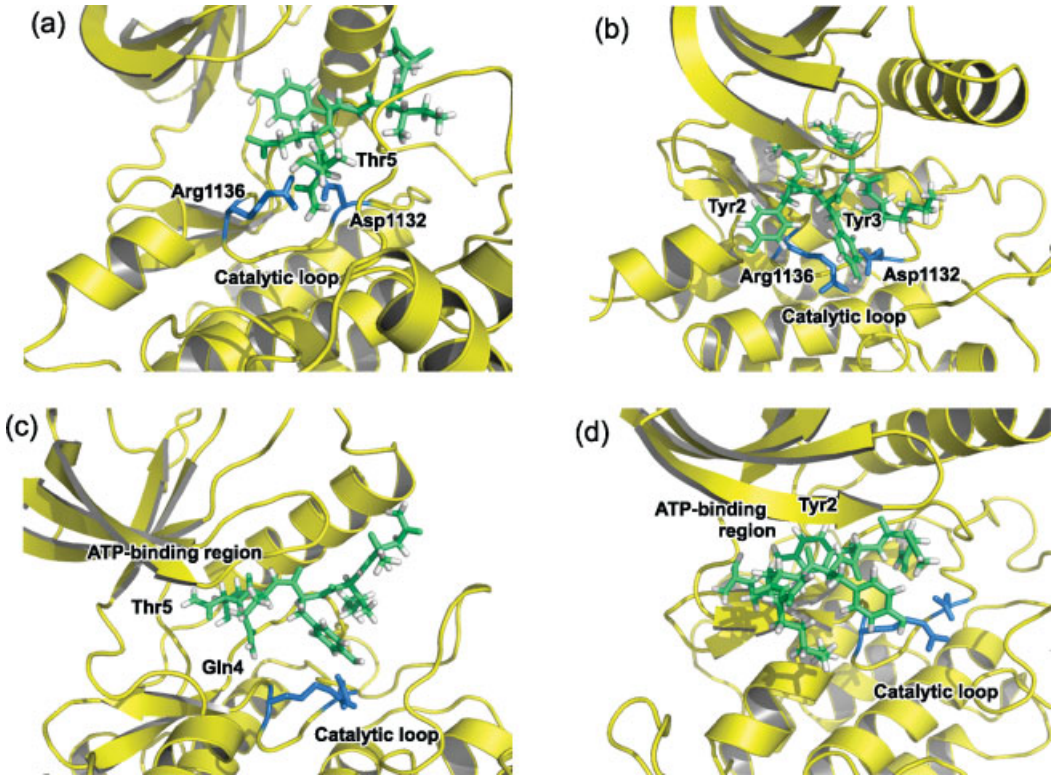

Figure 8. Proposed binding models of (a) DIYET, (b) DYYRK, (c) NIYQT, and (d) NYYRK for the kinase domain of IR (IRK) calculated using AMBER scoring function. The backbone of IRK is displayed as a ribbon model in yellow and the side chains of catalytic Asp1132 and Arg1136 are displayed as stick models in blue. The peptides are displayed as stick models in green.

a crucial role in the interaction with IR. The inhibitory effect of DpYpYRK was much weaker than that of its parent peptide, DYYRK (Figure 2), while the inhibitory potency of DIpYET was comparable to that of DIYET. Tyr/pTyr-substituted peptides include amino-acid sequences of the phosphorylated activation loop. In particular, DpYpYRK includes the crucial phosphotyrosine, i.e. pTyr1162, which is predominantly phosphorylated [33]. It is thought that the peptide was repelled from the catalytic loop in the kinase domain like the phosphorylated activation loop. These results suggest that DYYRK behaves as an autoinhibition region, i.e. the activation loop [15–17] despite its short length. On the other hand, DIpYET includes pTyr1158, which is secondarily phosphorylated by IR; therefore, the inhibitory potency of DIEYT was little affected by Tyr/pTyr substitution.

These peptides have amino-acid sequences around the autophosphorylation sites of IR, and we anticipated that the peptides would bind to the substrate-binding site of IR. The most favorable amino-acid sequence of a substrate recognized by IR has been identified [34]. The sequence, XEEEYMMMM (X is an arbitrary amino acid), includes multiple negatively charged amino acids on the *N*-terminal side of phosphorylatable tyrosine. The negative charges are assumed to be essential to interacting with positively charged amino acids around the substrate-binding site in the kinase domain [35]. On the basis of this assumption, we predicted that the replacement of negatively charged amino acids in inhibitory peptides with uncharged amino acids [i.e. the replacement of aspartate with asparagine (Asp/Asn) or of glutamate with glutamine (Glu/Gln)] would prevent the peptides from binding to IR and reduce the inhibitory effect. Contrary to our prediction, the inhibitory effects of the modified peptides (NIYQT and NYYRK) were greater than those of their parent peptides (Figure 3). A similar observation was found in the previous study on the inhibitory peptides of EGFR [36]. These results suggest that negatively charged amino-acid residues in the peptides are not involved in the inhibition or that the binding site of NIYQT and NYYRK in IR is different from that of the parent peptides.

In order to investigate this suggestion, we examined the effects of the concentration of ATP on the inhibitory potencies of peptides. While the inhibitory potencies of DIYET and DYYRK were not affected by the concentration of ATP (Figure 1), those of NIYQT and NYYRK were affected (Figure 3). These results indicate that NIYQT and NYYRK are ATP-competitive inhibitors and DIYET and DYYRK are not; therefore, NIYQT and NYYRK are thought to bind to the ATP-binding region in the kinase domain, which is surrounded by nonpolar amino acids [16]. NIYQT and NYYRK are less polarized than DIYET and DYYRK. Hence, it is suggested that NIYQT and NYYRK could be accessible to the ATP-binding region. On the other hand, DIYET and DYYRK are not thought to interact with the ATP-binding region. Moreover, the results obtained from mass spectrometry indicate that these peptides are phosphorylated by IR (Table 1 and Figure 5); therefore, DIYET and DYYRK are suggested to behave as a substrate, that is, they would interact with the catalytic loop in the kinase domain, which catalyzes phosphotransfer reactions. In mass spectrometry, it was found that NIYQT is phosphorylated by IR (Table 2) although it is suggested to be an ATP-competitive inhibitor (Figure 3). NIYQT would interact with both the ATP-binging region and the catalytic loop. Hence, NIYQT is expected to inhibit the autophosphorylation of IR mainly in an ATP-competitive manner and partly in a

Journal of PeptideScience

substrate-competitive manner, and might contribute to the lower IC_{50} value of NIYQT (24.6 μM) more than those of the other peptides.

Non-ATP-competitive inhibitors can more selectively inhibit the activity of target proteins than ATP-competitive inhibitors [37]. Therefore, non-ATP-competitive inhibitory peptides, DIYET and DYYRK, are presumed to inhibit the autophosphorylation of IR selectively. In order to confirm this presumption, we estimated the effects of inhibitory peptides on the autophosphorylation of EGFR, one of the most common RTKs. DIYET hardly inhibited the autophosphorylation of EGFR and the inhibitory effect of DYYRK was less than that on IR (Figure 4). In contrast, the inhibitory effects of NIYQT and NYYRK on the autophosphorylation of EGFR were comparable to that on IR (Figure 4). ATP-competitive inhibitors, NIYQT and NYYRK, had less selectivity for IR, as expected. On the other hand, an inhibitory peptide, which is not an ATP-competitive inhibitor, DIYET and DYYRK, would preferentially inhibit IRK rather than that of other RTKs.

We carried out computational simulations in order to obtain more knowledge on the inhibition mechanism. DOCK Suite of Programs 6 was used to estimate interactions between IRK and the inhibitory peptides. NIYQT and NYYRK were located on the ATP-binding pocket (Figure 8(c) and (d)). This result coincides with the experimental results that NIYQT and NYYRK inhibited the autophosphorylation of IR in an ATP-competitive manner. DIYET and DYYRK were located near the catalytic loop (Figure 8(a) and (b)). These results reflect the experimental results that these peptides are not ATP-competitive inhibitors and might interact with the catalytic loop. The docking program has had modest success in predicting which small molecule drugs bind to proteins [38]. The inhibitory peptides appear to be larger than small molecule drugs used in the test cases for DOCK; however, the program predicted that ATP-competitive inhibitors, NIYQT and NYYRK, would bind to the ATP-binding region in IRK, whereas non-ATP-competitive inhibitors, DIYET and DYYRK, would bind to another site (Figure 8). Thus, our results obtained from docking simulations are thought to be reasonable.

Although ATP-competitive inhibitors of tyrosine kinases are popular, substrate-competitive inhibitors have more benefits [37,39] as they are less likely to inhibit other targets because the substrate-binding site is less conserved than the ATP-binding region. Moreover, a substrate-competitive inhibitor does not need to compete with the very high intracellular concentration of ATP (~5000 μM) [40], which leads to the requirement for a high concentration of an ATP-competitive inhibitor for *in vivo* activities [41]. Thus, substrate-competitive inhibitors are suitable for the development of drugs with fewer adverse effects. Indeed, DIYET and DYYRK, which are not ATP-competitive inhibitors, would preferentially inhibit the kinase activity of IR rather than that of EGFR, whereas NIYQT and NYYRK competing with ATP inhibit the autophosphorylation of EGFR (Figure 4).

Although the inhibitory effect of DIYET on the autophosphorylation of IR was reported in our previous study, the inhibition mechanism has not been proved. In this study, we obtained more knowledge about this mechanism. It was found that DIYET is not an ATP-competitive inhibitor and employs a novel mechanism. DYYRK also inhibited the autophosphorylation of IR, suggesting that it employs the same mechanism as DIYET. Moreover, the potent inhibitory effect of NIYQT is not negligible, although the peptide is an ATP-competitive inhibitor. More studies on these peptides could lead to the development of a novel peptidic drug.

References

1 Schlessinger J. Cell signaling by receptor tyrosine kinases. *Cell* 2000; **103**: 211–225.
2 Blume-Jensen P, Hunter T. Oncogenic kinase signaling. *Nature* 2001; **411**: 355–365.
3 Al-Obeidi A, Wu1 JJ, Lam KS. Protein tyrosine kinases: structure, substrate specificity, and drug discovery. *Biopolymers* 1998; **47**: 197–223.
4 Levitzki A, Gazit A. Tyrosine kinase inhibition: an approach to drug development. *Science* 1995; **267**: 1782–1788.
5 Lee J, Pilch PF. The insulin receptor: structure, function, and signaling. *Am. J. Physiol.* 1994; **266**: C319–C334.
6 White MF, Shoelson SE, Keutmann H, Kahn CR. A cascade of tyrosine autophosphorylation in the β-subunit activates the phosphotransferase of the insulin receptor. *J. Biol. Chem.* 1988; **263**: 2969–2980.
7 Skolnik EY, Batzer A, Li N, Lee C-H, Lowenstein E, Mohammadi M, Margolis B, Schlessinger J. The function of GRB2 in linking the insulin receptor to Ras signaling pathways. *Science* 1993; **260**: 1953–1955.
8 Saltiel AR, Kahn CR. Insulin signaling and the regulation of glucose and lipid metabolism. *Nature* 2001; **414**: 799–806.
9 Hubbard SR, Mohammadi M, Schlessinger J. Autoregulatory mechanisms in protein-tyrosine kinases. *J. Biol. Chem.* 1998; **273**: 11987–11990.
10 Shewchuk LM, Hassell AM, Ellis B, Holmes WD, Davis R, Horne EL, Kadwell SH, McKee DD, Moore JT. Structure of the Tie2 RTK domain: self-inhibition by the nucleotide binding loop, activation loop, and C-terminal tail. *Structure* 2000; **8**: 1105–1113.
11 Chiara F, Bishayee S, Heldin C-H, Demoulin J-B. Autoinhibition of the platelet-derived growth factor beta-receptor tyrosine kinase by its C-terminal tail. *J. Biol. Chem.* 2004; **279**: 19732–19738.
12 Meyer RD, Singh AJ, Rahimi N. The carboxyl terminus controls ligand-dependent activation of VEGFR-2 and its signaling. *J. Biol. Chem.* 2004; **279**: 735–742.
13 Yokoyama N, Ischenko I, Hayman MJ, Miller WT. The C terminus of RON tyrosine kinase plays autoinhibitory role. *J. Biol. Chem.* 2005; **280**: 8893–8900.
14 Wybenga-Groot LE, Baskin B, Ong SH, Tong J, Pawson T, Sicheri F. Structural basis for autoinhibition of the Ephb2 receptor tyrosine kinase by the unphosphorylated juxtamembrane region. *Cell* 2001; **106**: 745–757.
15 Hubbard SR, Wei L, Ellis L, Hendrickson WA. Crystal structure of the tyrosine kinase domain of the human insulin receptor. *Nature* 1994; **372**: 746–754.
16 Hubbard SR. Crystal structure of the activated insulin receptor tyrosine kinase in complex with peptide substrate and ATP analog. *EMBO J.* 1997; **16**: 5572–5581.
17 Ablooglu AJ, Frankel M, Rusinova E, Ross JBA, Kohanski RA. Multiple activation loop conformations and their regulatory properties in the insulin receptor's kinase domain. *J. Biol. Chem.* 2001; **276**: 46933–46940.
18 Hirose M, Kuroda Y, Sawa S, Nakagawa T, Hirata M, Sakaguchi M, Tanaka Y. Suppression of insulin signalling by a synthetic peptide KIFMK suggests the cytoplasmic linker between DIII-S6 and DIV-S1 as a local anaesthetic binding site on the sodium channel. *Br. J. Pharmacol.* 2004; **142**: 222–228.
19 Berman HM, Westbrook J, Feng Z, Gilliland G, Bhat TN, Weissig H, Shindyalov IN, Bourne PE. The Protein Data Bank. *Nucleic Acids Res.* 2000; **28**: 235–242.
20 DeLano WL. PyMOL: an open-source molecular graphics tool. *PPC4 Newsl. Prot. Crystallogr.* 2002; **40**: 11.
21 Pettersen EF, Goddard TD, Huang CC, Couch GS, Greenblatt DM, Meng EC, Ferrin TE. UCSF Chimera – a visualization system for exploratory research and analysis. *J. Comput. Chem.* 2004; **25**: 1605–1612.
22 Cornell WD, Cieplak P, Bayly CI, Gould IR, Merz KM Jr, Ferguson DM, Spellmeyer DC, Fox T, Caldwell JW, Kollman PA. A second generation force field for the simulation of proteins, nucleic acids, and organic molecules. *J. Am. Chem. Soc.* 1995; **117**: 5179–5197.
23 Kuntz ID. Structure-based strategies for drug design and discovery. *Science* 1992; **257**: 1078–1082.
24 Kuntz ID, Meng EC, Shoichet BK. Structure-based molecular design. *Acc. Chem. Res.* 1994; **27**: 117–123.

25 Shoichet BK, Bodian DL, Kuntz ID. Molecular docking using shape descriptors. *J. Comput. Chem.* 1992; **13**: 380–397.
26 Meng EC, Shoichet BK, Kuntz ID. Automated docking with grid-based energy evaluation. *J. Comput. Chem.* 1992; **13**: 505–524.
27 Ewing TJA, Makino S, Skillman AG, Kuntz ID. DOCK4.0: search strategies for automated molecular docking of flexible molecule databases. *J. Comput. Aided Mol. Des.* 2001; **15**: 411–428.
28 Kollman PA, Massova I, Reyes C, Kuhn B, Huo S, Chong L, Lee M, Lee T, Duan Y, Wang W, Donini O, Cieplak P, Srinivasan J, Case DA, Cheatham TE III. Calculating structures and free energies of complex molecules: combining molecular mechanics and continuum models. *Acc. Chem. Res.* 2000; **33**: 889–897.
29 Onufriev A, Bashford D, Case DA. Exploring protein native states and large-scale conformational changes with a modified generalized born model. *Proteins* 2004; **55**: 383–394.
30 Mills JEJ, Dean PM. Three-dimensional hydrogen-bond geometry and probability information from a crystal survey. *J. Comput. Aided Mol. Des.* 1996; **10**: 607–622.
31 Ward WH, Cook PN, Slater AM, Davies DH, Holdgate GA, Green LR. Epidermal growth factor receptor tyrosine kinase: investigation of catalytic mechanism, structure-based searching and discovery of a potent inhibitor. *Biochem. Pharmacol.* 1994; **48**: 659–666.
32 Paonessa F, Foti D, Costa V, Chiefari E, Brunetti G, Leone F, Luciano F, Wu F, Lee AS, Gulletta E, Fusco A, Brunetti A. Activator protein-2 overexpression accounts for increased insulin receptor expression in human breast cancer. *Cancer Res.* 2006; **66**: 5085–5093.
33 Wei L, Hubbard SR, Hendrickson WA, Ellis L. Expression, characterization, and crystallization of the catalytic core of the human insulin receptor protein-tyrosine kinase domain. *J. Biol. Chem.* 1995; **270**: 8122–8130.
34 Songyang Z, Carraway KL III, Eck MJ, Harrison SC, Feldman RA, Mohammadi M, Schlessinger J, Hubbard SR, Smith DP, Eng C, Lorenzo MJ, Ponder BAJ, Mayer BJ, Cantley LC. Catalytic specificity of protein-tyrosine kinases is critical for selective signalling. *Nature* 1995; **373**: 536–539.
35 Niv MY, Rubin H, Cohen J, Tsirulnikov L, Licht T, Peretzman-Shemer A, Cna'an E, Tartakovsky A, Stein I, Albeck S, Weinstein I, Goldenberg-Furmanov M, Tobi D, Cohen E, Laster M, Ben-Sasson SA, Reuveni H. Sequence-based design of kinase inhibitors applicable for therapeutics and target identification. *J. Biol. Chem.* 2004; **279**: 1242–1255.
36 Abe M, Kuroda Y, Hirose M, Kato M, Murakami M, Watanabe Y, Nakano M, Handa T. Inhibition of autophosphorylation of epidermal growth factor receptor by a small peptide not employing an ATP-competitive mechanism. *Biopolymers* 2008; **89**: 40–51.
37 Levitzki A. Protein kinase inhibitors as a therapeutic modality. *Acc. Chem. Res.* 2003; **36**: 462–469.
38 Warren GL, Andrews CW, Capelli A-M, Clarke B, LaLonde J, Lambert MH, Lindvall M, Nevins N, Semus SF, Senger S, Tedesco G, Wall ID, Woolven JM, Peishoff CE, Head MS. A critical assessment of docking programs and scoring functions. *J. Med. Chem.* 2006; **49**: 5912–5931.
39 Levitzki A, Mishani E. Tyrphostins and other tyrosine kinase inhibitors. *Annu. Rev. Biochem.* 2006; **75**: 93–109.
40 Traut TW. Physiological concentrations of purines and pyrimidines. *Mol. Cell. Biochem.* 1994; **140**: 1–22.
41 Lawrence DS, Niu J. Protein kinase inhibitors: the tyrosine-specific protein kinases. *Pharmacol. Ther.* 1998; **77**: 81–114.

